The Layered Structure of Coronary Adventitia under Mechanical Load

Huan Chen,[†] Yi Liu,[†] Mikhail N. Slipchenko,[‡] Xuefeng Zhao,[†] Ji-Xin Cheng,[‡] and Ghassan S. Kassab[†§*]
[†]Department of Biomedical Engineering, Indiana University-Purdue University-Indianapolis, Indianapolis, Indiana; [‡]Department of Biomedical Engineering, Purdue University, West Lafayette, Indiana; and [§]Departments of Surgery and Cellular and Integrative Physiology, Indiana University-Purdue University-Indianapolis, Indianapolis, Indiana

ABSTRACT The mechanical loading-deformation relation of elastin and collagen fibril bundles is fundamental to understanding the microstructural properties of tissue. Here, we use multiphoton microscopy to obtain quantitative data of elastin and collagen fiber bundles under in situ loading of coronary adventitia. Simultaneous loading-imaging experiments on unstained fresh coronary adventitia allowed morphometric measurements of collagen and elastin fibril bundles and their individual deformation. Fiber data were analyzed at five different distension loading points (circumferential stretch ratio $\lambda_\theta = 1.0$, 1.2, 1.4, 1.6, and 1.8) at a physiological axial stretch ratio of $\lambda_{axial} = 1.3$. Four fiber geometrical parameters were used to quantify the fibers: orientation angle, waviness, width, and area fraction. The results show that elastin and collagen fibers in inner adventitia form concentric densely packed fiber sheets, and the fiber orientation angle, width, and area fraction vary transmurally. The extent of fiber deformation depends on the initial orientation angle at no-distension state ($\lambda_\theta = 1.0$ and $\lambda_{axial} = 1.3$). At higher distension loading, the orientation angle and waviness of fibers decrease linearly, but the width of collagen fiber is relatively constant at $\lambda_\theta = 1.0$–1.4 and then decrease linearly for $\lambda_\theta \geq 1.4$. A decrease of the relative dispersion (SD/mean) of collagen fiber waviness suggests a heterogeneous mechanical response to loads. This study provides fundamental microstructural data for coronary artery biomechanics and we consider it seminal for structural models.

INTRODUCTION

Because the elastin and collagen fibers are the major mechanical microstructural elements of the blood vessel wall, knowledge of their morphology and deformation is fundamental to understanding vascular mechanical response. In the adventitia, dense and wavy collagen fibers form an interwoven network that tangles with elastin fibers and fibroblasts (1). Histologically, a collagen or elastin fiber can be described as a bundle of loosely bounded fibrils (2,3). In an undulating state, such a fiber can deform under a very small load. When straightened, it can sustain a significant amount of axial stress. Therefore, fibers are gradually straightened and begin to take up the increasing loads when the artery is distended (4). Clearly, the elastin and collagen fibers play a major role in the mechanical response of blood vessels (5–9).

Much effort has been made to relate the mechanical properties of tissues to the behavior and deformation of the microstructure (elastin and collagen fibers); i.e., to develop microstructure-based models for prediction of mechanical response of blood vessels subject to physiological or pathological loads (10–16). The majority of these constitutive models simplifies the microstructure and assumes fibers to be symmetrically disposed with respect to the axis of the vessel, with a preferred orientation, yielding macroscopic orthotropic constitutive law for each layer. The engagements of fibers (fibers become straight to take up load) are typically assumed to be governed by exponential functions (11–14). Other models assume the geometrical features of fibers follow a typical continuous distribution such as β-distribution with primarily planar array (10,15–17). The lack of accurate quantitative data of microstructure and deformation of elastin and collagen fibers in previous models is a barrier to accurately predicting a vessel microenvironment that may help clarify the initiation, progression, and clinical treatment of diseases such as atherosclerosis (18). Therefore, the quantitative data on geometry and deformation of fibers under physiological or pathological loads are needed for both understanding the morphology of vascular tissues and the development of accurate mechanical modeling.

The complexity of the microstructure, however, presents both imaging and computational challenges. Previous attempts to determine morphometric features, such as collagen and elastin fiber diameters, lengths, number density, orientations, and waviness, generally employed destructive differential digestion techniques (7,19). Such techniques have failed to provide accurate data other than the total mass density, because such methods change the physiological environment of tissues and affect fiber morphology. Recently, the development of nonlinear imaging modality (multiphoton microscopy, MPM) has enabled noninvasive measurements of biological tissues and cells. MPM imaging is driven by two primary types of nonlinear interaction between ultrafast laser light and biological tissues—two-photon excited fluorescence (TPEF) and second-harmonic generation (SHG).

In brief, TPEF is used to depict elastin that contains endogenous fluorophores, whereas the SHG signal originates

Submitted July 11, 2011, and accepted for publication October 31, 2011.

*Correspondence: gkassab@iupui.edu

Editor: Charles Wolgemuth.

0006-3495/11/12/2555/8 $2.00

doi: 10.1016/j.bpj.2011.10.043

from collagen type I that contains molecular noncentrosymmetric structures. MPM is well developed and widely implemented for imaging cells (20–22), thin tissue sections (23,24), thick unstained biological specimens (4,25), and engineered tissues (26,27). Zoumi et al. (4) studied the microstructure (collagen and elastin fibers) of fixed artery specimens using SHG and TPEF to determine the deformation of fibers under different fixed distension conditions. Arkill et al. (25), on unstained and unfixed collecting lymphatic vessels, combined SHG, TPEF, and coherent anti-Stokes Raman scattering to visualize the cellular and extracellular responses to mechanical loads. Unfortunately, no quantitative data were presented in this recent study.

The objective of this article was to quantify the geometrical data of the collagen and elastin fibers of arterial wall under in situ deformation. To this end, unstained fresh adventitia specimens of left anterior descending (LAD) arteries were imaged simultaneously under various mechanical loading, and the in situ deformation of elastin and collagen fibers was measured for a given fiber. Statistical analysis was also carried out to describe the population of fibers in terms of geometrical features such as orientation angle, waviness, width, and area fraction. These data establish a microstructural foundation for vascular biomechanics, and may lead to a better understanding of vascular function and dysfunction.

MATERIALS AND METHODS

Adventitia preparation

The hearts of healthy pigs ($n = 7$, body weight in the range of 80–90 Kg) were obtained at a local slaughterhouse. The hearts were transported to the laboratory in 4°C physiological solution (0.9% NaCl) within 1 h after the animals were sacrificed. The LAD arteries were dissected carefully from their emergence at aortic ostia, and the adjacent tissue around the segments was dissected carefully in physiological solution. The LAD arteries were then inverted (turned inside-out), and the exposed intima-media layers were peeled off carefully. Removal of the intima-media is relatively easy and does not damage the adventitia layer (28), as external elastic laminae exist that structurally separate the media and adventitia layers (1). In preliminary studies, it was found that thickness of the adventitia layer of porcine LAD artery is ~100–150 μm, where the loose tissue (outer adventitia) accounts for ~70 μm or more. Due to the limitation in the penetration depth of the MPM, and because it is impossible to thoroughly remove the loose tissue of adventitia layer, we scanned the adventitia specimens from the media-adventitia surface by inverting the adventitia. Because the adventitia at no-load state is rather loose and the opening angle is relatively small (29), the mechanical deformation is not significantly altered by the inversion.

Multiphoton microscopy

MPM images from the adventitia specimen were obtained using a combined SHG/TPEF setup, which consists of a mode-locked Ti:Sapphire laser (Chameleon Vision; Coherent, Santa Clara, CA) and an upright optical microscope (Olympus America, Center Valley, PA). The average excitation power at the sample was ~40 mW with an excitation wavelength of 830 nm. The TPEF and SHG signals were collected by the same objective and directed toward two external photomultiplier-tube (PMT) detectors. The dichroic mirror (750dcxr; Chroma Technology, Brattleboro, VT) was used to separate detected signals from the excitation beam. For simultaneous imaging, the SHG signal from collagen at 415 nm and TPEF signal from elastin at ~520 nm were separated from each other and directed toward two external PMTs by dichroic mirror (425dcxr; Chroma). The corresponding bandpass filters (405/40 and 520/40 from Chroma) was used in front of PMTs to selectively detect SHG and TPEF signals.

It is noted that the fluorescent microsphere was also two-photon excited by 830-nm beam. Only a small portion of very strong signal from fluorescent microspheres (emission wavelength 584 nm) passed through 520/40 nm bandpass filter and appeared in TPEF images. A 60× 1.1NA water immersion objective (LUMFI; Olympus America) was used for all specimens, and each acquired image (with resolution of ~0.23 μm/pixel) covered an area of 120 × 120 μm^2 and was integrated over two frames to improve the signal/noise ratio. Images were obtained starting from the top of the sample surface toward the inner sample (outer adventitia) in the z direction; i.e., at various depths of the adventitia wall. The step size between slices was typically set at 0.25 μm, and the number of slices for one site was limited to 160 due to the penetration depth. The scan time for an entire Z stack was <5 min. The total scan time for a set of loading conditions was <1 h.

Distension protocol

Mechanical testing

A straight segment of the adventitia was cut ~1 cm in length, and every branch bifurcation was identified and ligated to eliminate leakage. Mechanical tests were first conducted on a motor-controlled triaxial testing machine (28,29) for determination of diameter-pressure curve of the adventitia (Table 1). The specimens were axially stretched with longitudinal (axial) stretch ratio $\lambda_{axial} = 1.3$ to mimic physiological conditions for pig coronary arteries (30). The luminal pressure P was increased gradually from 0 to 140 mmHg. The specimen was preconditioned to axial stretch and pressure several times to ensure repeatable data.

MPM scanning

The segment was removed from the triaxial machine and kept in cold physiological solution. The MPM imaging was performed within 24 h after harvest. A custom-made organ bath-chamber device (Fig. 1) was used. The setup contained a subchamber in which a specimen vessel segment was mounted within a round chamber to protect the microscope system from possible overflow of solution in the subchamber. A horizontal micromanipulator was fixed in the chamber device to stretch the vessel segment axially (Fig. 1, *left*). The specimen was first mounted on cannulae in the subchamber and immersed in physiological solution, and stretched to in vivo length ($\lambda_{axial} = 1.3$) by the left micromanipulator. The chamber device was then mounted on the stage of an upright microscope, and a custom-made elastic balloon tip catheter was inserted into the lumen of vessel through the subchamber cannulae with the other end connected to a syringe pump controlled by a micromanipulator (Fig. 1, *right*). The elastic balloon was inflated or deflated when moving the right micromanipulator axially to distended the specimen to the desired diameter. The elastic balloon was used to avoid microvibration and movement induced by possible leakage through

TABLE 1 The average luminal pressures in simultaneous loading-imaging experiments were determined by the circumferential stretch ratio λ_θ according to diameter-pressure curves of specimens

λ_θ	1.0	1.2	1.4	1.6	1.8
Pressure (mmHg)	0	4.06 ± 0.32	8.06 ± 0.71	16.2 ± 3.05	148 ± 24.5

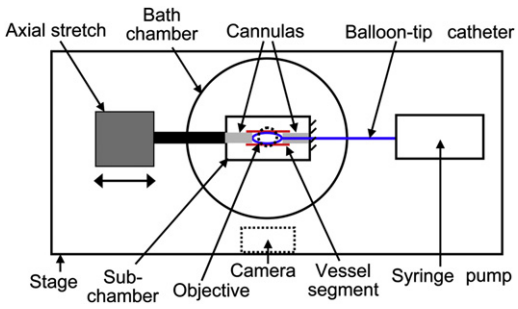

FIGURE 1 Schematic diagram of the experimental setup.

the thin adventitia if inflation was made directly with physiological solution. The use of a balloon maintained the lateral and axial movement of the adventitia specimen <<0.25 μm during MPM imaging. A commercial camera (model No. T1i; Canon, Lake Success, NY) with a macro lens ($f =$ 100 mm) was used to record the diameter of specimen (D) (Fig. 1, *bottom*), and the corresponding distension loading condition was determined by circumferential stretch ratio λ_θ of the specimen with initial diameter D_0 in no-distension state as the reference; i.e., $\lambda_\theta = D/D_0$.

A number of 10-μm diametrical fluorescent microspheres with rhodamine B (excitation wavelength of 540 nm and emission wavelength of 584 nm) were used as markers to track the scan area as well as the deformation of individual fiber under various mechanical loads. To begin, the microspheres were randomly dispersed on the outer surface of the specimen after the specimen was mounted. Because the inflated elastic balloon was shuttlelike rather than cylindrical, we focused on the top of the distended specimen (usually in the middle of specimen, as shown in Fig. 2, *a–c*). A photo of the specimen with a scaling marker was taken by the camera before MPM imaging to record the specimen diameter (Fig. 2, *a–c*). While imaging, these microspheres appeared in TPEF images with elastin fibers (Fig. 2, *d–i*) and formed the basis for the scan area.

To obtain accurate deformation of fibers, an area with microspheres at four edges was selected. This area preferably contained <4–6 microspheres to avoid excessive covering of fibers. Images with lower magnification were captured first to ensure the scan area was always focused in the middle of microspheres (Fig. 2, *d–f*). The TPEF and SHG images with higher magnification were then collected simultaneously (Fig. 2, *g–l*). When increasing distention load, the elastic balloon was inflated slowly to follow the scan area at all times during the scan. Five mechanical loading conditions were considered: $\lambda_\theta = 1.0$, 1.2, 1.4, 1.6, and 1.8. Specifically, seven specimens were scanned at no-distension state ($\lambda_\theta = 1.0$ and $\lambda_{axial} = 1.3$) to obtain morphometric data of collagen and elastin fibers, of which five specimens were further scanned at various loading conditions.

Image processing and statistical analysis

The elastin and collagen were found to form multiple concentric densely packed fiber sheets, with thickness of 3–7 mm and alternating principle directions. Due to the highly scattering nature of the tissue, the MPM images became blurred beyond 30 μm depth of adventitia (Fig. 3 *a*). Hence, MPM images of only the first five layers of seven adventitia specimens were collected (total average thickness of 30 μm) to obtain clear images of adventitia microstructure. The representative image, usually in the middle of the layer, was then selected and systematically analyzed in each layer (Fig. 4). (Although the selected images show excellent signal/noise ratio, some collagen fibers coming out of the imaging plane in the z direction give a false impression of discontinuities in collagen networks (Fig. 3 *d*). Such discontinuities in collagen fibers may underestimate the waviness and area fraction; note that these cases were excluded from analysis.)

Image processing was then implemented on selected MPM images. To begin, the center-lines of individual fibers were drawn manually, and then

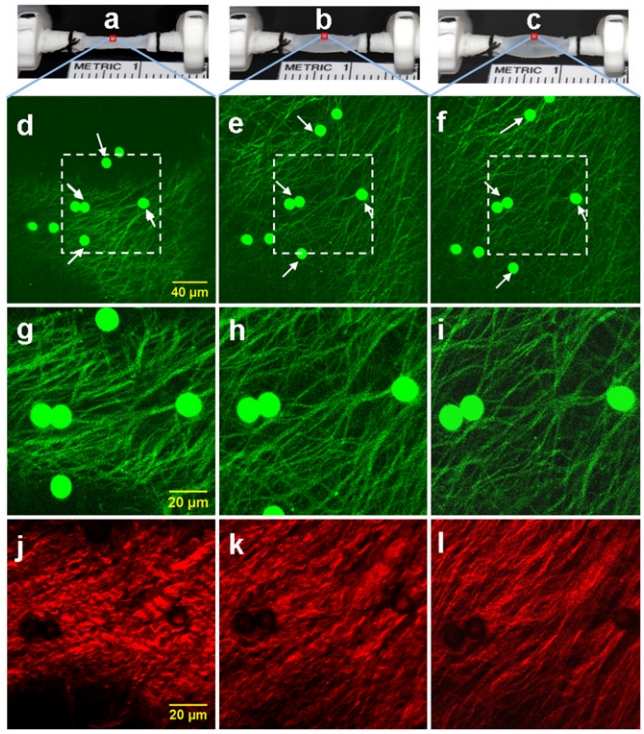

FIGURE 2 MPM images of collagen and elastin fibers under different mechanical loading. Fluorescent microspheres were used to track the scan area and deformation of individual fibers. (*a–c*) Photos of the specimen with the scaling marker in subchamber were taken to record the specimen diameters at (*a*) no-distension state $\lambda_\theta = 1.0$; (*b*) $\lambda_\theta = 1.63$; and (*c*) $\lambda_\theta =$ 1.92, respectively. (*d–f*) TPEF images with lower magnification were captured first to track the scan area at corresponding loads. (*g–i*) TPEF images (for elastin fiber) with appropriate magnification and resolution were collected at corresponding loads. (*j–l*) SHG images (for collagen fiber) were collected simultaneously with TPEF images.

smoothed through B-spline interpolation (Fig. 3 *b*) using MATLAB (The MathWorks, Natick, MA). Based on the center-line of the fiber, the following geometrical parameters were obtained: the orientation angle θ was determined by the angle between direction of linear fit center-line and circumferential direction of specimen, and the waviness λ_0 was determined by the ratio of total arc-length to end-to-end straight length of fiber (Fig. 3 *c*). The width D of a single fibril bundle was also measured directly in images. The MPM images were thresholded to separate background and fiber-containing pixels using a threshold value that was found to separate clearly distinguishable fibers from background and out-of-plane fibers. The area fractions of fibers C were determined by the ratio of total number of white/black pixels in thresholded images (Fig. 3 *d*).

Based on the above measurements, statistical analysis was used to describe the population of fibers in terms of the following morphometric features: the orientation angle θ, the waviness λ_0, the width D, and the area fraction of fibers C. Specifically, the mean and distribution rates of geometrical parameters at the no-distension state were determined. The population of geometrical parameters of individual fibers was calculated in each layer, and the mean parameter was obtained by averaging over a total of 35 layers (seven specimens). To determine the distribution pattern, the populations of geometrical parameters of all layers were grouped together. Furthermore, the change of these morphometric features at various loading points was also obtained. The average geometrical parameter of a specimen layer was considered as an independent statistical sample, and the parameter was averaged over five layers of each specimen ($n = 5$) at five different mechanical loading points ($\lambda_\theta = 1.0$, 1.2, 1.4, 1.6, 1.8), respectively. The

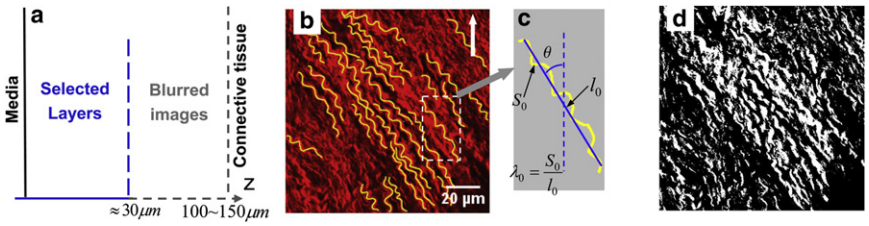

FIGURE 3 (*a*) Selected fiber layers were within ≈30 μm depth of inner adventitia. (*b*) Center-lines of fibers on a MPM image (*arrow* indicates the circumferential direction). (*c*) The orientation angle θ and the waviness λ_0 for a single fiber. (*d*) Threshold of MPM image to a binary image for measurement of the area fraction of fibers.

results were expressed as means ± SE. The significance of the differences between the variables under various mechanical loading was evaluated by one-way ANOVA test. The results were considered statistically different when $P < 0.05$.

RESULTS

Morphometric data of elastin and collagen fibers at no-distension state

Layered structure

Both elastin and collagen fibers in inner adventitia formed layered structures, where orientation, width, and area fraction of fibers revealed significant transmural variation as shown in Fig. 4. Such sublayer structure was ~3–7 mm thick and occupied 30–40% of the total adventitial thickness. This structure was not present toward the exterior adventitia where collagen fibers were highly random and elastin fibers were largely absent.

Orientation angle

In each adventitia layer, there was a main orientation of collagen and elastin fibers (varies along the adventitia wall, *white arrows* in Fig. 4), and a secondary principle direction for elastin fibers (*yellow arrows* in Fig. 4). The orientation angles of collagen fibers followed a bell-shaped distribution (truncated normal distribution) in each layer, expressed by the exponential function: $\%population = \mathrm{Exp}(-ax^2 - b)$, with a and b indicating width and height of the bell, respectively (Table 2). Furthermore, the main orientation angles varied in subsequent layers randomly as shown in Fig. 4. The orientation distribution of collagen fibers of all 35 layers from seven specimens was shown in Fig. 5 *a*, which demonstrated that most collagen fibers aligned at ~60 (circumferential direction $\theta = 0^\circ$ and axial direction $\theta = 90^\circ$) in the no-distension state, and the main orientation angles of elastin fibers were parallel with collagen fibers but with secondary principle directions. This near-axial orientation is likely due to the axial loading but no pressure (i.e., no distension state). When the vessel was pressurized and axially stretched, the fiber orientation angle decreased and oriented in the circumferential direction.

Waviness

The waviness of the collagen fibril bundle was also found to follow a bell-shaped distribution as shown in Fig. 5 *b* (mean waviness is ~1.23). The morphometric features of elastin fiber differed significantly from collagen where elastin was rodlike rather than a spiral, and >80% of elastin fiber was straight (waviness $\lambda_0 \approx 1.0$) at no-distension state (Fig. 4, *f–j*). For both elastin and collagen fibers, the waviness did not vary significantly in different layers.

Width and area fraction

It was found that collagen fibers became thicker toward the exterior of adventitia, whereas elastin fibers became thinner as shown in Fig. 5 *c* (mean width of fibers over seven specimens in each layer). The width-layer relationships of fibers were curve-fitted using linear regression. It can be seen that the width of collagen changed more than that of elastin in inner adventitia. The average width of collagen fibers of all layers was ~2.8 μm, and that of elastin fibers was 2.0 μm. Similarly, the area fraction of collagen fibers was found to

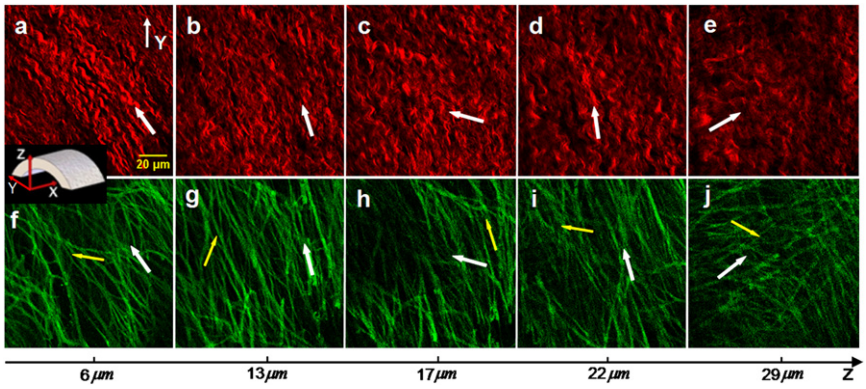

FIGURE 4 Both collagen and elastin fibers in inner adventitia form layered structures. Images *a–e* are five collagen layers at different depth *Z*, and images *f–j* are five elastin layers at the exactly same depth. (*White arrow*) Main orientation of fibers in all layers. (*Yellow arrow*) Second principle direction for elastin (*X*, *Y*, *Z*: axial, circumferential, and radial directions) in all layers.

TABLE 2 In each layer, the orientation angles of collagen fibers were found to follow a bell-shaped distribution: %*population* = Exp($-ax^2 - b$) with *a* and *b* as the width and height of the bell, respectively

Loads λ_θ	Maximum value (%)	a	b	R^2
1.0	22.8	16.0	1.71	0.92
1.2	26.7	21.9	1.54	0.99
1.4	28.4	23.3	1.51	0.90
1.6	30.5	37.1	1.39	0.87
1.8	35.1	47.6	1.20	0.93

Parameters a and b were determined by least-squares fit of measured data (ranged from $-40°$ to $40°$). The bell-shape distribution became narrower and sharper (increased a and reduced b) with increase of loading.

increase significantly in deeper layers whereas that of elastin fibers decreased moderately as shown in Fig. 6. The average area fraction of collagen and elastin over all layers were 33% and 22%, respectively.

In situ deformation of elastin and collagen fibers

In situ deformation of individual fibers under various mechanical loading points was tracked in reference to the fluorescent microspheres (Fig. 2). It was found that the extent of fiber deformation depended upon the initial orientation angle at no-distension state. Fibers oriented toward the circumferential direction (distension direction) were stretched much more than those aligned more axially, such that the former became straightened or thinner earlier than the latter. For collagen fibers, the orientation angle and the waviness were approximately uniform in a layer so that fiber deformation tended to be homogeneous (Fig. 2, *j–l*), whereas elastin fiber deformation was much more heterogeneous due to the various fiber orientations (Fig. 2, *g–i*). Analysis for each geometrical parameter was made as outlined below.

Orientation angle

Both collagen and elastin fibers gradually oriented toward the circumferential direction (Fig. 5 *d*). The orientation-distension relationships of collagen and elastin were curve-fitted by a linear least-squares method. Because collagen fibers aligned uniformly in a layer, the change of their mean orientation angles was more homogeneous, whereas the orientation angles of elastin were heterogeneous with multiple directions as shown in Fig. 5 *d*; i.e., the orientation of collagen shifted toward the circumferential direction more gradually than the elastin fibers. Furthermore, collagen fibers in a layer tended to align toward the principal direction so that the bell-shape distribution of orientation angles became narrower with increased a and reduced b, as shown in Table 2.

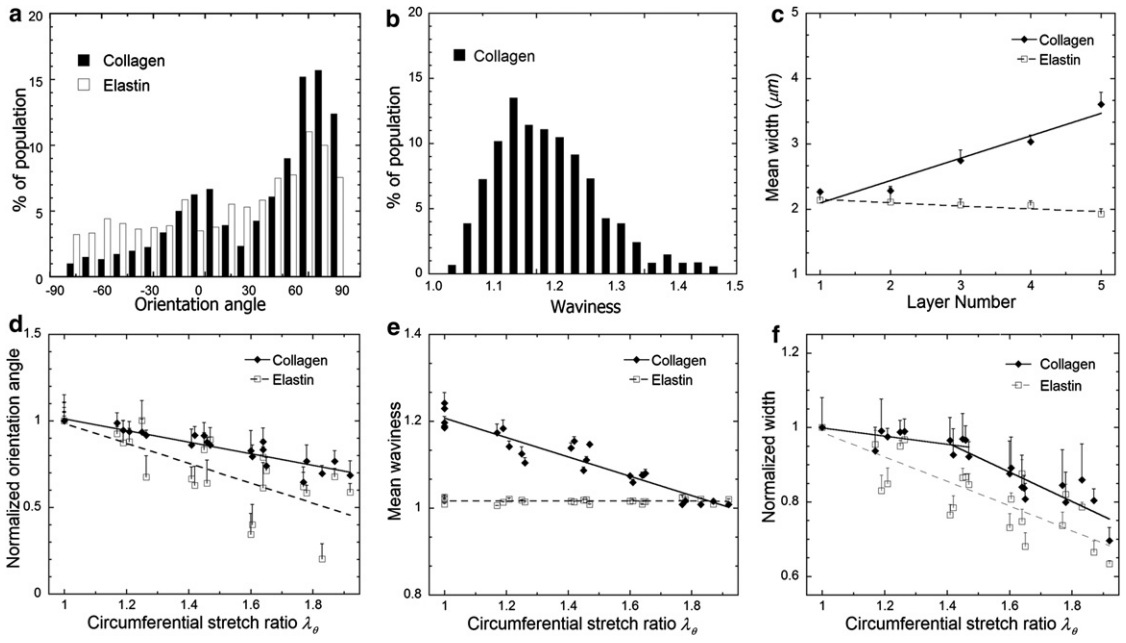

FIGURE 5 Statistical data of microstructure and deformation of collagen and elastin fibers. At no-distention state ($\lambda_\theta = 1.0$ with axial stretch ratio $\lambda_{axial} = 1.3$): (*a*) The orientation distribution of fibers of all specimen layers. (*b*) The bell-shaped distribution of the collagen fiber waviness of all layers. (*c*) Layer-to-layer heterogeneity of the fiber width. The curve-fitted linear width-layer relationship of collagen is 1.76 + 0.34N (correlation coefficient $R = 0.97$, N is the layer number), and that of elastin is 2.20–0.05N ($R = 0.92$). At different higher loadings: (*d*) Change of mean orientation angle normalized by initial orientation angle at $\lambda_\theta = 1.0$, and fitted linear orientation-distension relationship of collagen fibers is 1.35–0.34λ_θ ($R = 0.94$), and that of elastin fibers is 1.56–0.58λ_θ ($R = 0.78$). (*e*) Change of mean waviness, and fitted linear waviness-distension relationship of collagen fibers is 1.43–0.22 λ_θ ($R = 0.95$) and waviness of elastin fibers is ~1.0 constantly. (*f*) Change of mean width normalized by initial width at $\lambda_\theta = 1.0$, and fitted width-distension relationship of collagen is a piecewise function: 1.11–0.10 λ_θ ($R = 0.70$ and $P > 0.05$) when $1.0 \le \lambda_\theta < 1.4$ and 1.51–0.40 λ_θ ($R = 0.88$) when $1.4 \le \lambda_\theta \le 1.6$; and fitted linear width-distension relationship of elastin fibers is 1.32–0.33 λ_θ ($R = 0.87$).

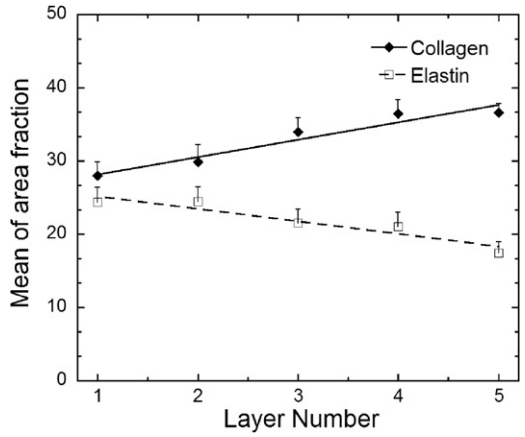

FIGURE 6 Layer-to-layer heterogeneity of area fraction of collagen and elastin fibers at no-distension state ($\lambda_\theta = 1.0$ with axial stretch ratio $\lambda_{axial} = 1.3$), and curve-fitted area fraction-layer relationship of collagen is 25.8 + 2.38N ($R = 0.97$) and that for elastin fibers is 27.0–1.73N ($R = 0.95$).

Waviness

In Fig. 5 *e*, a linear least-squares fit was used to describe the waviness-distension relation of collagen, which showed that the collagen fibers were stretched gradually at elevated distension and became completely straightened ($\lambda_0 \approx 1.0$) to take up loads at $\lambda_\theta \approx 1.8$ (as shown in Fig. 2 *i*). Although the initial waviness of collagen fiber slightly varied in different layers, the waviness became uniform under higher loads. As shown in Fig. 5 *e* (*error bars* are smaller under higher loads), the relative dispersion ($RD = SD$/mean) of waviness of collagen fiber decreased gradually with increase of loading conditions (i.e., $RD = 6.0–2.9\ \lambda_\theta$; $R = 0.78$, and $P < 0.05$). This suggests that the layered structure adventitia has a heterogeneous mechanical response to loads given the observed significant transmural heterogeneity. It should be noted that the RDs of orientation angle and width of fibers were independent of circumferential loads.

Width

The change of collagen width was more homogeneous than that of elastin fiber (Fig. 5 *f*) consistent with the change of fiber orientation angle. The width change of collagen fibers was insignificant at lower loading ($\lambda_\theta = 1.0$, 1.2, and 1.4, and $P > 0.05$), but decreased at $\lambda_\theta > 1.4$ ($P < 0.05$); hence, a piecewise linear function was used to describe the width-distension relationship of collagen fibers. On the other hand, elastin fibers became thinner continuously and gradually at higher loading, as shown in Fig. 5 *f*.

The statistical analysis above (Fig. 5, *d–f*) was based on fiber population rather than individual fibers. To validate these data, the deformation of 20 single fibers, which were randomly selected from five deformed samples (as identified by fluorescent spheres), was measured and then compared with the curve-fitted parameter-distension curves (Fig. 7). The results showed that the deformation data of statistical population and individual single fibers were consistent at physiological conditions.

DISCUSSION

The morphometric analysis of adventitia microstructure shows that both elastin and collagen fibers form layered structures consistent with those found in the literature (19,31) and some of their geometric features change transmurally. The orientation angles of fibers change significantly between layers but most remain on the same quadrant of circumferential direction. This differs from previous studies on other vascular tissue that suggest the fiber orientations are uniformly distributed over the whole azimuthal range using destructive techniques (31,32). It was also found that elastin fibers are oriented parallel to the collagen fibers with an additional minor principle orientation. Hence, the elastin fibers scatter over the whole azimuthal space (in contrast to collagen, which has a preferred alignment in the no-distension state). As a result, elastin fibers form a netlike structure, and collagen fibers tend to align, uniformly, in a layer. This confirms the assumption that noncollagenous matrix material (including elastin fibers) is associated with an isotropic mechanical response of vessel wall, whereas anisotropic deformation is almost entirely due to collagen fibers in most models (11–15).

The width and area fraction of collagen fibers increase toward the external adventitia whereas that of elastin fibers were found to decline gradually as shown in Fig. 5 *c* and Fig. 6. The elastin fibers were rarely found in exterior adventitia where collagen fibers become much thicker and orient randomly. The outer adventitia occupies ~60–70% of adventitia thickness and the main function of thicker collagen fibers is to support the vessel and connect with surrounding tissue rather than to resist the transmural pressure. On the other hand, the inner adventitia, which consists of alternating elastin and collagen fiber layers, plays an important role in opposing the transmural pressure and prevents overdistension of vessel at high loading. A microstructure-based model (15) can allow consideration of the protective function of adventitia of coronary arteries with the present measured geometry and deformation of microstructures, allowing accurate prediction of both macroscopic responses and the microenvironment of a blood vessel.

To our knowledge, this is the first study that documents direct in situ deformation of individual fibers under various distension loads. The fiber deformation was found to strongly depend upon the initial orientation angle of a fiber. The nearly uniform alignment of collagen fibers makes their deformation more homogeneous than elastin fibers, which have multiple directions in each layer. As a result, collagen fibers were uniformly stretched and shifted toward the circumferential direction of adventitia (Fig. 2, *j–l*), and elastin fibers gradually resembled a network (Fig. 2, *g–i*).

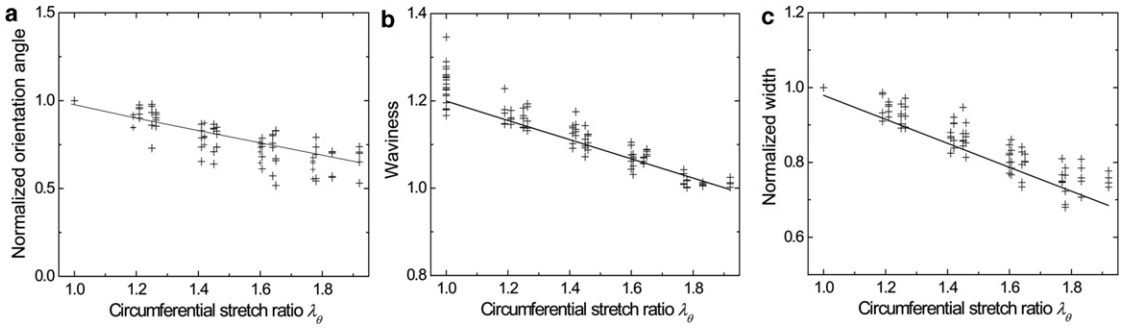

FIGURE 7 Statistical quantitative analysis of fiber deformation (*solid lines*) is validated by deformation of 20 individual fibers (*small crosses*). (*a*) Change of normalized orientation angles of individual collagen fibers is consistent with previous curve-fitted linear function 1.35–0.34 λ_θ. (*b*) Change of the waviness of individual collagen fibers is consistent with previous curve-fitted linear function 1.43–0.22 λ_θ. (*c*) Change of normalized width of individual elastin fibers is consistent with previous curve-fitted linear function 1.32–0.33 λ_θ.

Additionally, change of the fiber orientation and waviness depends on both the longitudinal stretch and luminal pressure. The statistical data (Fig. 5 *a*) showed that most of the elastin and collagen fibers oriented themselves toward the axial direction rather than the circumferential direction at no-distension state with physiological axial stretch ratio $\lambda_{axial} = 1.3$. When the specimens were returned to their relaxed axial length with luminal pressure remaining zero, elastin and collagen fibers reoriented and aligned in the circumferential direction (25), and collagen fibers became slightly more undulated.

The collagen fibers thinned down significantly (Fig. 5 *f*) at $\lambda_\theta \approx 1.4$, albeit they were not completely straightened at this state. This is consistent with the diameter-pressure curve of coronary adventitia that shows the adventitia becomes stiffer after $\lambda_\theta \approx 1.4$ (Table 1). In other words, collagen fibers in adventitia were gradually recruited after $\lambda_\theta \approx 1.4$ to take up loads, and then gradually predominate in the mechanical function of adventitia and became completely straightened when loaded at $\lambda_\theta \approx 1.8$. This finding suggests that collagen contributes mainly to the flat region of the nonlinear stress-strain curve whereas elastin mainly contributes to the toe-portion of the stress-strain curve (4,5). This underscores the idea that the function of the adventitia in a normal vessel (with physiological blood pressure $\lambda_\theta \approx 1.5$) is to support the vessel, not take up loads.

All of the deformation patterns were described by linear least-squares fit as shown in Fig. 5, *d–f*. However, these linear relationships were only determined between distension loading $\lambda_\theta = 1.0$ to $\lambda_\theta = 1.8$. When considering distension loading beyond $\lambda_\theta = 1.8$, these relationships may become nonlinear. For instance, because collagen fibers became completely straightened ($\lambda_0 \approx 1.0$) at $\lambda_\theta = 1.8$, the waviness of collagen fibers did not change further, and remained 1.0 at higher loading $\lambda_\theta \geq 1.8$. Similarly, the change of orientation angle of collagen and elastin fibers decreased when they approached the circumferential direction. In future studies, a larger range of loading should be considered to determine the extent of linearity.

There were other limitations that warrant mention: First, it was observed that some collagen fibers were out of the imaging plane in the z direction and formed coils; i.e., three-dimensional helix structures (25), which resulted in a false impression of discontinuities of collagen networks in the two-dimensional images. Therefore, the two-dimensional image processing available as of this writing may underestimate some of the geometrical features of collagen fibers (e.g., for the waviness and area fraction) and any apparent discontinuities were excluded from measurements. This limitation suggests the need, in the future, for three-dimensional reconstruction of fibers that can render a more-accurate morphology of fibers in vascular tissue. Second, manual image processing was implemented on selected two-dimensional images to obtain quantitative data of individual fiber orientation angle, waviness, and width. However, manual measurement is inefficient and time-consuming. Therefore, the development of an automated segmentation and image processing algorithm is necessary to avoid manual measurement error and to speed up data collection.

CONCLUSIONS

To our knowledge, this is the first study that provides quantitative data on microstructure and in situ deformation of both elastin and collagen fibers of blood vessel adventitia. The distribution patterns and layer-to-layer heterogeneity of fibers reflect what we believe to be realistic microstructures of adventitial wall and will, in our opinion, contribute to future models of blood vessels. The observed heterogeneous mechanical response to various distension states will lead to a better understanding of vascular biomechanics. In future studies, the stress and strain relationship of an individual fiber should be determined to predict both macro- and microscopic mechanical response of blood vessels.

This research was supported by the National Institutes of Health-National Heart, Lung, and Blood Institute grant R01HL087235-03.

REFERENCES

1. Rhodin, J. A. G. 1979. Architecture of the vessel wall. *In* Handbook of Physiology, *Vol. 2*. R. M. Berne, editor. American Physiology Society, Bethesda, MD: Sect. 2, 1–31.
2. Fratzl, P., K. Misof, …, S. Bernstorff. 1998. Fibrillar structure and mechanical properties of collagen. *J. Struct. Biol.* 122:119–122.
3. Ottani, V., M. Raspanti, and A. Ruggeri. 2001. Collagen structure and functional implications. *Micron.* 32:251–260.
4. Zoumi, A., X. Lu, …, B. J. Tromberg. 2004. Imaging coronary artery microstructure using second-harmonic and two-photon fluorescence microscopy. *Biophys. J.* 87:2778–2786.
5. Roach, M. R., and A. C. Burton. 1957. The reason for the shape of the distensibility curves of arteries. *Can. J. Biochem. Physiol.* 35:681–690.
6. Oka, S. 1972. Some theoretical studies on hemorheology. *In* Advances in Biophysics, *Vol. 3*. M. Kotani, editor. University of Tokyo, Tokyo, Japan. 97.
7. Oka, S., and T. Azuma. 1970. Physical theory of tension in thick-walled blood vessels in equilibrium. *Biorheology.* 7:109–117.
8. Azuma, T., and S. Oka. 1971. Mechanical equilibrium of blood vessel walls. *Am. J. Physiol.* 221:1310–1318.
9. Azuma, T., and M. Hasegawa. 1971. A rheological approach to the architecture of arterial walls. *Jpn. J. Physiol.* 21:27–47.
10. Lanir, Y. 1983. Constitutive equations for fibrous connective tissues. *J. Biomech.* 16:1–12.
11. Holzapfel, G. A., and T. C. Gasser. 2000. A new constitutive framework for arterial wall mechanics and a comparative study of material models. *J. Elast.* 61:1–48.
12. Zulliger, M. A., P. Fridez, …, N. Stergiopulos. 2004. A strain energy function for arteries accounting for wall composition and structure. *J. Biomech.* 37:989–1000.
13. Kroon, M., and G. A. Holzapfel. 2008. A new constitutive model for multi-layered collagenous tissues. *J. Biomech.* 41:2766–2771.
14. Li, D., and A. M. Robertson. 2009. A structural multi-mechanism constitutive equation for cerebral arterial tissue. *Int. J. Solids Struct.* 46:2920–2928.
15. Chen, H., Y. Liu, …, G. S. Kassab. 2011. A micromechanics finite-strain constitutive model of fibrous tissue. *J. Mech. Phys. Solids.* 59:1823–1837.
16. Hollander, Y., D. Durban, …, Y. Lanir. 2011. Experimentally validated microstructural 3-D constitutive model of coronary arterial media. *J. Biomech. Eng. Mar.* 133:031007.
17. Lokshin, O., and Y. Lanir. 2009. Micro and macro rheology of planar tissues. *Biomaterials.* 30:3118–3127.
18. Vito, R. P., and S. A. Dixon. 2003. Blood vessel constitutive models—1995–2002. *Annu. Rev. Biomed. Eng.* 5:413–439.
19. Haas, K. S., S. J. Phillips, …, J. V. White. 1991. The architecture of adventitial elastin in the canine intrarenal aorta. *Anat. Rec.* 230:86–96.
20. Campagnola, P. J., H. A. Clark, …, L. M. Loew. 2001. Second-harmonic imaging microscopy of living cells. *J. Biomed. Opt.* 6: 277–286.
21. Gauderon, R., P. B. Lukins, and C. J. Sheppard. 2001. Optimization of second-harmonic generation microscopy. *Micron.* 32:691–700.
22. Mansfield, J., J. Yu, …, P. Winlove. 2009. The elastin network: its relationship with collagen and cells in articular cartilage as visualized by multiphoton microscopy. *J. Anat.* 215:682–691.
23. Campagnola, P. J., A. C. Millard, …, W. A. Mohler. 2002. Three-dimensional high-resolution second-harmonic generation imaging of endogenous structural proteins in biological tissues. *Biophys. J.* 82: 493–508.
24. Garcia, M., and G. S. Kassab. 2009. Right coronary artery becomes stiffer with increase in elastin and collagen in right ventricular hypertrophy. *J. Appl. Physiol.* 106:1338–1346.
25. Arkill, K. P., J. Moger, and C. P. Winlove. 2010. The structure and mechanical properties of collecting lymphatic vessels: an investigation using multimodal nonlinear microscopy. *J. Anat.* 216:547–555.
26. Zoumi, A., A. Yeh, and B. J. Tromberg. 2002. Imaging cells and extracellular matrix in vivo by using second-harmonic generation and two-photon excited fluorescence. *Proc. Natl. Acad. Sci. USA.* 99: 11014–11019.
27. Raub, C. B., J. Unruh, …, S. C. George. 2008. Image correlation spectroscopy of multiphoton images correlates with collagen mechanical properties. *Biophys. J.* 94:2361–2373.
28. Wang, C., M. Garcia, …, G. S. Kassab. 2006. Three-dimensional mechanical properties of porcine coronary arteries: a validated two-layer model. *Am. J. Physiol. Heart Circ. Physiol.* 291:H1200–H1209.
29. Lu, X., A. Pandit, and G. S. Kassab. 2004. Biaxial incremental homeostatic elastic moduli of coronary artery: two-layer model. *Am. J. Physiol. Heart Circ. Physiol.* 287:H1663–H1669.
30. Liu, Y., W. Zhang, …, G. S. Kassab. 2011. A linearized and incompressible constitutive model for arteries. *J. Theor. Biol.* 286:85–91.
31. Finlay, H. M., L. McCullough, and P. B. Canham. 1995. Three-dimensional collagen organization of human brain arteries at different transmural pressures. *J. Vasc. Res.* 32:301–312.
32. Smith, J. F. H., P. B. Canham, and J. Starkey. 1981. Orientation of collagen in the tunica adventitia of the human cerebral artery measured with polarized light and the universal stage. *J. Ultrastruct. Res.* 77: 133–145.